Optimal Sliding Mode Control for Spacecraft Rendezvous with Collision Avoidance

Licheng Feng, Qing Ni, Yuzhu Bai*, Xiaoqian Chen, Yong Zhao
College of Aerospace Science and Engineering, National University of Defense Technology
Changsha, Hunan, China

Abstract— **In this paper, the problem of relative motion control of spacecraft close-range rendezvous without collision on elliptical orbit is considered. An autonomous amalgamated control algorithm is presented to deal with the nonlinear dynamics problem with external disturbances. This new control scheme combines the efficiency of the optimal sliding mode control (OSMC) (used for attraction towards goal position) and the collision avoidance capability of the artificial potential function (APF) method (used for repulsion from moving obstacle). The nonlinear optimal control strategy is based on infinite-horizon state-dependent Riccatic equation (SDRE). For ensuring robustness of the optimal controller in presence of parametric uncertainty and external disturbances, a sliding mode control scheme is realized by combining an integral and a terminal sliding surface. The APF controller takes velocity of both the chaser and obstacle into consideration. Using the Lyapunov stable theory, the stability of the closed-loop system is guaranteed. Numerical simulation results are presented to verify the effectiveness and capability of the proposed control scheme.**

I. INTRODUCTION

A rendezvous space mission can be divided into several phases: launch, phasing, far range rendezvous, close-range rendezvous and docking [1]. In the past decades, the problems related to autonomous rendezvous and docking have been well developed and applied to many space missions. The close-rendezvous can be divided into two sub phases: a preparatory phase leading to the final approach corridor, usually called "closing"[1], and a final approach phase leading to the docking condition. The close-rendezvous mission often presents several control challenges: in order to achieve soft and safe docking, the approaching speed of the chase vehicle should be very slow to avoid physical damage with the target and other obstacles. What's more, the tracking errors in relative position and velocity should also be very small. To meet all these challenges, many different approaches have been investigated.

Optimal control theory is one of the most important branches in modern control theory and linear quadratic regulation (LQR) is a well understood and accepted theory upon which many modern controllers are based. Many literatures used the LQR control algorithm to solve the rendezvous problem [2, 3] based on Hill-Clohessy-Wiltshire linearized equations. However, the CW dynamic equations are simplified; the chaser spacecraft relative motion in close-range maneuvers is governed by highly nonlinear kinematics and dynamics between the target and chaser spacecraft. Now we have the option of using an extension of LQR theory on nonlinear problems known as State-Dependent Riccati Equation (SDRE) nonlinear regulation [4]. In the past decades, the SDRE method has been developed to offer a systematic and effective means for designing nonlinear controllers [5, 6] and introduced to the field of spacecraft rendezvous and formation flying. For instance, Stansbery and Cloutier [7] proposed a SDRE-based method to control the position and attitude of a spacecraft in the proximity of a tumbling target. Mauro and Mattia [8] applicated SDRE technique to spacecraft formation flying. In the SDRE control algorithm, nonlinear equations of motion are represented in a linear-like form, called the state-dependent coefficient (SDC) form, which corresponds to the system matrix expressed explicitly as a function of the state element.

Sliding mode control (SMC) [9] was proposed in the beginning of 1970 and it has been widely recognized as a powerful control strategy for nonlinear uncertain systems due to its simplicity and inherent robustness towards the matched uncertainty. This control method has been used to the field of spacecraft formation flying and rendezvous [10-13].

A typical SMC is conservatively designed for the worst case scenario in which the system uncertainties and external disturbances are dominant. In such circumstance, stability is the main concern of SMC design. However, most real physical systems are more or less transparent to us with only a small portion of uncertainties. Once the system nominal part is dominant, robustness is no longer the only concern of control design. Criteria like minimizing control input, achieving faster convergence to the equilibrium state should be taken into consideration.

It is well known that optimal control provides a systematic design methodology which makes the designed controller optimal according to the performance index. But the main limitation of optimal or suboptimal control is the requirement of complete system knowledge or the sensitivity to system uncertainties or external perturbations. A possible solution to this problem is to introduce SMC into optimal control whenever uncertainties are present. This control strategy optimal sliding mode control (OSMC) [14, 15] can make optimal control more robust and applicable to systems with

*Corresponding author. Email: baiyuzhu@hotmail.com
Project supported by the National Natural Science Foundation of China (NO. 11302253)

978-1-5090-0623-6/16/$31.00 ©2016 IEEE

uncertainties. Active research is continuing in the field of OSMC in continuous as well as discrete domain[16-18].

To deal with obstacle constraints, artificial potential field (APF) method is a good choice. The APF method has been maturely applied in a wide variety of systems, including terrestrial based robots, spacecraft and autonomous road vehicles [19-21]. APF method involves the creation of a scalar-valued, nonnegative artificial potential function in workspace of the system. The APF has its global minimum at the desired location of the system. Typically, an APF is composed from the superposition of two types of functions: attractive potentials and repulsive potentials. The attractive potential is a bow-shaped function whose global minimum is the goal point. The repulsive potential has large value near obstacles and small or zero value far from obstacles.

In the past years, many researches successfully applied the APF method to autonomous proximity operations of spacecraft, spacecraft formation flying missions and on-orbit autonomous assembly [22-24]. Josue D. Munoz [25] created an adaptive artificial potential function methodology for rapid path-planning of spacecraft autonomous proximity operations. Gao Peng et al. [26] researched on the adaptive artificial potential function guidance for dynamic obstacle avoidance. Besides, some researches on the combination of LQR method and APF method also have been conducted [27]. Leonel Palacios et al. [24] designed an autonomous distributed LQR/APF control algorithm for cube-sat swarms maneuvering and the dynamic model was based on Tschauner and Hempel (TH) equations. Shawn B. McCamish and Marcello Romano [28] designed a LQR/APF control algorithm and proved its efficiency through the hardware test on SPHERES.

The objective of this paper is to develop a control algorithm which combines the efficiency of OSMC with the collision avoidance capability of APF-based concepts. The APF-based collision avoidance relies on relative position and velocity, rather than only on position, for controlling spacecraft. In addition, the new designed APF control law was deduced based on that of the static avoidance, which means the new guidance law can deal with dynamic obstacle problems. The stability of the proposed APF control algorithm is proved through the Lyapunov stable theory.

The paper is organized as follows. In section II, relative dynamics model of rendezvous is described. The OSMC/APF control scheme is presented in section III, and it includes two parts: the spacecraft OSMC control algorithm and the spacecraft APF control algorithm. In section IV, numerical results and analysis based on the proposed controller are presented. The paper is then concluded with a summary section in section V.

II. System Dynamics

This section presents the development of nonlinear relative dynamics for eccentric orbits. Two spacecraft orbiting around the Earth is considered. One of the spacecraft is called target and the other is called chaser. The Earth Centered Inertial (ECI) coordinate system and the Local Vertical Local Horizontal (LVLH) coordinate system are used to describe the motion dynamics.

The inertial position of the target is denoted as $\boldsymbol{r}_t$ and the position of the chaser is expressed by $\boldsymbol{r}_c$ in ECI frame. The dynamics of the target and chaser in the inertial frame can be written as

$$\begin{cases} \dfrac{d^2\boldsymbol{r}_c}{dt^2} = -\dfrac{\mu \boldsymbol{r}_c}{r_c^3} + \boldsymbol{u}_c + \boldsymbol{d}_c \\ \dfrac{d^2\boldsymbol{r}_t}{dt^2} = -\dfrac{\mu \boldsymbol{r}_t}{r_t^3} + \boldsymbol{u}_t + \boldsymbol{d}_t \end{cases} \tag{1}$$

where μ is the Earth gravity constant, $\boldsymbol{u}$ is control vector, $\boldsymbol{d}$ is the vector of bounded external disturbance acceleration. The disturbances include the Earth oblateness J_2 effect, third body gravity effects, aerodynamic drag, solar radiation pressure etc. In this study, only the Earth oblateness J_2 effect and aerodynamic drag are included. The relative perturbation acceleration due to the J_2 effect in the LVLH frame is described as [29]

$$\Delta \boldsymbol{a}_{J_2} = 6\frac{J_2 \mu R_e^2}{r_t^5}\begin{bmatrix} 1-3\sin^2 i \sin^2 u & \sin^2 i \sin 2u & \sin 2i \sin u \\ \sin^2 i \sin 2u & -\frac{1}{4}-\sin^2 i(\frac{1}{2}-\frac{7}{4}\sin^2 u) & -\frac{1}{4}\sin 2i \cos u \\ \sin 2i \sin u & -\frac{1}{4}\sin 2i \cos u & -\frac{3}{4}+\sin^2 i(\frac{1}{2}+\frac{5}{4}\sin^2 u) \end{bmatrix} \tag{2}$$

where $J_2 = 0.0010826$, $R_e = 6378.1366\text{m}$ is the radius of the Earth, i is the inclination angle and u is argument of latitude.

The atmospheric drag perturbation acceleration is first expressed in the ECI coordinates

$$\boldsymbol{a}_d = -\frac{1}{2}\rho\left(\frac{C_d A}{m}\right)\|\boldsymbol{v}\|\boldsymbol{v} \tag{3}$$

where m is the mass of spacecraft, A is the effective surface, C_d is the drag coefficient, ρ is the local atmospheric density, $\boldsymbol{v}$ is the spacecraft velocity vector relative to the atmosphere. Then we transform the atmospheric drag perturbation into the LVLH frame. The exact relative atmospheric drag perturbation acceleration $\Delta \boldsymbol{a}_d$ can be obtained from [29].

Therefore, the sum of all disturbance acceleration is given by

$$\boldsymbol{d} = \Delta \boldsymbol{a}_{J_2} + \Delta \boldsymbol{a}_d \tag{4}$$

It is assumed that only the chaser spacecraft is controlled, hence $\boldsymbol{u}_t = \boldsymbol{0}$. The relative position of the chaser with respect to the target is $\boldsymbol{r} = \boldsymbol{r}_c - \boldsymbol{r}_t$ and it is assumed that $\|\boldsymbol{r}\| << \|\boldsymbol{r}_t\|$ under the gravitational attraction of a main body. Then relative dynamics can be expressed as

$$\frac{d^2\boldsymbol{r}}{dt^2} = \frac{d^2\boldsymbol{r}_c}{dt^2} - \frac{d^2\boldsymbol{r}_t}{dt^2} = -\frac{\mu \boldsymbol{r}_c}{r_c^3} + \frac{\mu \boldsymbol{r}_t}{r_t^3} + \boldsymbol{u}_c + \boldsymbol{d}_c - \boldsymbol{d}_t \tag{5}$$

According to the knowledge between the absolute motion and the relative motion, the relative acceleration in the ECI frame can be measured in the LVLH frame:

$$\frac{d^2\boldsymbol{r}}{dt^2}=\frac{\delta^2\boldsymbol{r}}{\delta t^2}+2\boldsymbol{\omega}\times\frac{\delta\boldsymbol{r}}{\delta t}+\boldsymbol{\omega}\times(\boldsymbol{\omega}\times\boldsymbol{r})+\boldsymbol{\varepsilon}\times\boldsymbol{r} \tag{6}$$

where $\frac{\delta\boldsymbol{r}}{\delta t}$ and $\frac{\delta^2\boldsymbol{r}}{\delta t^2}$ are relative velocity and relative acceleration of the chaser spacecraft in the LVLH coordinate respectively. $\boldsymbol{\omega}$ and $\boldsymbol{\varepsilon}$ are rotational angular velocity vector and the rotational angular acceleration vector respectively. We define $\boldsymbol{x}=[\,\boldsymbol{r}^T\ \dot{\boldsymbol{r}}^T\,]^T$, therefore the nonlinear relative dynamics is described as [30]

$$\dot{\boldsymbol{x}}=f(\boldsymbol{x})+B(\boldsymbol{x})\boldsymbol{u}+B(\boldsymbol{x})\boldsymbol{d} \tag{7}$$

where

$$f(\boldsymbol{x})=\begin{bmatrix}\dot{x}\\ \dot{y}\\ \dot{z}\\ 2\dot{\theta}\dot{y}+\dot{\theta}^2x+\ddot{\theta}y+\dfrac{\mu}{r_t^2}-\dfrac{\mu(r_t+x)}{r_c^3}\\ -2\dot{\theta}\dot{x}+\dot{\theta}^2y-\ddot{\theta}x-\dfrac{\mu y}{r_c^3}\\ -\dfrac{\mu z}{r_c^3}\end{bmatrix} \tag{8}$$

$$B(\boldsymbol{x})=\begin{bmatrix}\boldsymbol{0}_{3\times3}\\ I_{3\times3}\end{bmatrix} \tag{9}$$

$$\dot{\theta}=\left[\frac{\mu(1+e\cos\theta)}{r_t^3}\right]^{1/2}\qquad \ddot{\theta}=-\frac{2\mu e\sin\theta}{r_t^3} \tag{10}$$

e, θ are the eccentricity and the true anomaly of the reference target orbit , respectively.

III. Control Strategy Design

The developed control strategy is a combination of OSMC and APF. The proposed control scheme combines desirable characteristics of OSMC and APF. It uses the OSMC response as the attractive force and the APF repulsion for collision avoidance. The OSMC method improves the performance of the control while the repulsive APF provides collision avoidance capability which OSMC cannot offer in a dynamic environment.

A. Optimal Sliding Mode Control

Optimal sliding mode control method consists of two parts: optimal control and sliding mode control. In the region dominated by the system nominal part, the system behavior is mainly governed by optimal control. In the region where perturbation becomes dominant, SMC will take over the main control task.

System (7) is a nonlinear dynamic system, the state dependent Riccati equation (SDRE) approach can be used to solve infinite-time nonlinear optimal control problem

$$\min J=\frac{1}{2}\int_0^\infty \boldsymbol{x}^TQ\boldsymbol{x}+\boldsymbol{u}^TR\boldsymbol{u}dt \tag{11}$$

subject to the relative dynamics of (7) with weight matrices $Q\ge\boldsymbol{0}$ and $R>\boldsymbol{0}$.

The SDRE design method uses direct parameterization to bring the nonlinear system into SDC form, which is a linear-like structure

$$\begin{aligned}\dot{\boldsymbol{x}}&=A(\boldsymbol{x})\boldsymbol{x}+B(\boldsymbol{x})\boldsymbol{u}\\ f(\boldsymbol{x})&=A(\boldsymbol{x})\boldsymbol{x}\end{aligned} \tag{12}$$

There are many choices of $A(\boldsymbol{x})$. In this paper, it adapts the nonlinear item by dividing $\boldsymbol{r}^T\boldsymbol{r}$, then the particular choice of $A(\boldsymbol{x})$ for this application is given by

$$A(\boldsymbol{x})=\begin{bmatrix}\boldsymbol{0}_{3\times3} & I_{3\times3}\\ A_{21} & A_{22}\end{bmatrix} \tag{13}$$

where

$$A_{21}=\begin{bmatrix}\dot{\theta}^2-\dfrac{\mu}{r_c^3}+a_{11} & \ddot{\theta}+a_{12} & a_{13}\\ -\ddot{\theta} & \dot{\theta}^2-\dfrac{\mu}{r_c^3} & 0\\ 0 & 0 & -\dfrac{\mu}{r_c^3}\end{bmatrix} \tag{14}$$

$$\begin{aligned}a_{11}&=\left(\frac{\mu}{r_t^2}-\frac{\mu}{r_c^3}r_t^2\right)x/\left(\boldsymbol{r}^T\boldsymbol{r}\right)\\ a_{12}&=\left(\frac{\mu}{r_t^2}-\frac{\mu}{r_c^3}r_t^2\right)y/\left(\boldsymbol{r}^T\boldsymbol{r}\right)\\ a_{13}&=\left(\frac{\mu}{r_t^2}-\frac{\mu}{r_c^3}r_t^2\right)z/\left(\boldsymbol{r}^T\boldsymbol{r}\right)\end{aligned} \tag{15}$$

$$A_{22}=\begin{bmatrix}0 & 2\dot{\theta} & 0\\ -2\dot{\theta} & 0 & 0\\ 0 & 0 & 0\end{bmatrix} \tag{16}$$

To obtain a valid solution of the SDRE, the pair $\{A(\boldsymbol{x}),B(\boldsymbol{x})\}$ has to be point-wise stabilized. From performance index (11), the optimal feedback control is given by

$$\boldsymbol{u}^*(\boldsymbol{x})=-R(\boldsymbol{x})^{-1}B(\boldsymbol{x})^TP(\boldsymbol{x})\boldsymbol{x}(t) \tag{17}$$

where $P(\boldsymbol{x})$ is the solution to the generalized SDRE

$$\begin{aligned}&P(\boldsymbol{x})A(\boldsymbol{x})+A(\boldsymbol{x})P(\boldsymbol{x})+Q(\boldsymbol{x})\\ &-P(\boldsymbol{x})B(\boldsymbol{x})R(\boldsymbol{x})^{-1}B(\boldsymbol{x})^TP(\boldsymbol{x})=\boldsymbol{0}\end{aligned} \tag{18}$$

so the closed-loop dynamics of system is expressed as

$$\dot{\boldsymbol{x}}(t)=\left(A(\boldsymbol{x})-R(\boldsymbol{x})^{-1}B(\boldsymbol{x})^TP(\boldsymbol{x})\right)\boldsymbol{x}(t) \tag{19}$$

According to the optimization theory, the closed-loop system (12) is asymptotically stable. However, due to the presence of perturbation, it is apparent that the motion will

wander the optimal trajectory. Therefore, we will utilize the optimal controller (17) to design an optimal sliding mode control law.

In this work, an integral sliding surface [18] is chosen:

$$\begin{aligned} \boldsymbol{s}(\boldsymbol{x},t) &= G[\boldsymbol{x}(t)-\boldsymbol{x}(0)] \\ &\quad - G\int_0^t \left(A(\boldsymbol{x})-R(\boldsymbol{x})^{-1}B(\boldsymbol{x})^T P(\boldsymbol{x})\right)\boldsymbol{x}(\tau)d\tau \end{aligned} \tag{20}$$

where $G = B^T$ and satisfies the non-singularity of GB.

Equivalent control law can be solved from $\dot{\boldsymbol{s}}(\boldsymbol{x},t) = \boldsymbol{0}$:

$$\boldsymbol{u}_{eq}(t) = -R(\boldsymbol{x})^{-1}B(\boldsymbol{x})^T P(\boldsymbol{x})\boldsymbol{x}(t) \tag{21}$$

To ensure the reachability of the specified sliding surface (20), we design the following SMC law:

$$\boldsymbol{u}_{sw}(t) = -(GB)^{-1}K|\boldsymbol{s}|^{\alpha}\,\mathrm{sgn}(\boldsymbol{s}) \tag{22}$$

$$\boldsymbol{u}_{osmc}(t) = \boldsymbol{u}_{eq}(t) + \boldsymbol{u}_{sw}(t) \tag{23}$$

where $K > \boldsymbol{0}$ is the gain matrix and α satisfies $0 < \alpha < 1$. The following candidate Lyapunov is selected

$$V_1 = \frac{1}{2}\boldsymbol{s}^T\boldsymbol{s} \tag{24}$$

and the time derivative of V_1 is

$$\begin{aligned} \dot{V}_1 &= \boldsymbol{s}^T(-K|\boldsymbol{s}|^{\alpha}\,\mathrm{sgn}(\boldsymbol{s}) + G\boldsymbol{d}) \\ &= |\boldsymbol{s}|(-K|\boldsymbol{s}|^{\alpha} + G\boldsymbol{d}\,\mathrm{sgn}(\boldsymbol{s})) \\ &\le |\boldsymbol{s}|(-K|\boldsymbol{s}|^{\alpha} + |G\boldsymbol{d}|) \end{aligned} \tag{25}$$

It is obvious that if K and α are chosen properly, then $\dot{V} < 0$ and the asymptotical stability of the closed-loop system can be guaranteed. In practice, sgn function can be replaced with continuous saturation function

$$sat(s_i, \varepsilon) = s_i / (|s_i| + \varepsilon) \tag{26}$$

B. Artificial Potential Function Control

During the maneuver of driving the chaser spacecraft from a state to another, it is possible to have some obstacle collisions in certain regions. Artificial Potential Function (APF) can be used to avoid obstacle collision.

An artificial potential is composed of the superposition of an attractive function and a series of impulsive functions. A typical choice for an attractive potential is a quadratic function

$$\phi_a = \frac{1}{2}(\boldsymbol{r}-\boldsymbol{r}_f)^T M(\boldsymbol{r}-\boldsymbol{r}_f) \tag{27}$$

where M is a symmetric positive definite matrix that shapes the attractive potential and $\boldsymbol{r}_f$ is the desired state. A typical way of defining repulsive potential function is using Gaussian function

$$\phi_r = \frac{1}{2}\sum_{i=1}^{N}\psi_i exp\left[-\frac{(\boldsymbol{r}-\boldsymbol{r}_{obsi})^T N_i(\boldsymbol{r}-\boldsymbol{r}_{obsi})}{\sigma_i}\right] \tag{28}$$

where $\boldsymbol{r}_{obsi}$ is the position of i^{th} obstacle in LVLH frame, ψ_i and σ_i are the height and width parameters, respectively, for the i^{th} repulsive potential and N_i is a positive definite matrix which shapes the i^{th} repulsive potential.

It is desired that an instantaneous force in the opposite direction of the local gradient of the artificial potential is applied when the rate of change of the artificial potential is positive [31]. In this essay, the method of velocity artificial potential function presented in reference [31] is adopted. However, we also take the velocities of multiple obstalces into consideration to design the control law.

We choose the Lyapunov candidate function similar to that adopted in reference [31]

$$V_2 = \frac{1}{2}(k\nabla_r\phi + \dot{\boldsymbol{r}})^T(k\nabla_r\phi + \dot{\boldsymbol{r}}) \tag{29}$$

Where k is a positive gain, and

$$\nabla_r\phi = M(\boldsymbol{r}-\boldsymbol{r}_f) - \sum_{i=1}^{N}\frac{\psi_i}{\sigma_i}exp\left[-\frac{(\boldsymbol{r}-\boldsymbol{r}_{obsi})^T N_i(\boldsymbol{r}-\boldsymbol{r}_{obsi})}{\sigma_i}\right]N_i(\boldsymbol{r}-\boldsymbol{r}_{obsi}) \tag{30}$$

The time derivative of V_2 is

$$\dot{V}_2 = (k\nabla_r\phi + \dot{\boldsymbol{r}})^T(k\nabla_r^T(\nabla_r\phi)\dot{\boldsymbol{r}} + k\nabla_{r_{obsi}}^T(\nabla_r\phi)\dot{\boldsymbol{r}}_{obsi} + \ddot{\boldsymbol{r}}) \tag{31}$$

where

$$\nabla_r^T(\nabla_r\phi) = M + \sum_{i=1}^{N}\frac{\psi_i}{\sigma_i^2}exp\left[-\frac{(\boldsymbol{r}-\boldsymbol{r}_{obsi})^T N_i(\boldsymbol{r}-\boldsymbol{r}_{obsi})}{\sigma_i}\right]\cdot \left[2N_i(\boldsymbol{r}-\boldsymbol{r}_{obsi})(\boldsymbol{r}-\boldsymbol{r}_{obsi})^T N_i - \sigma_i N_i\right] \tag{32}$$

$$\nabla_{r_{obsi}}^T(\nabla_r\phi) = -\sum_{i=1}^{N}\frac{\psi_i}{\sigma_i^2}exp\left[-\frac{(\boldsymbol{r}-\boldsymbol{r}_{obsi})^T N_i(\boldsymbol{r}-\boldsymbol{r}_{obsi})}{\sigma_i}\right]\cdot \left[2N_i(\boldsymbol{r}-\boldsymbol{r}_{obsi})(\boldsymbol{r}-\boldsymbol{r}_{obsi})^T N_i - \sigma_i N_i\right] \tag{33}$$

Since we use the OSMC response to replace the attractive force, the element M in $\nabla_r^T(\nabla_r\phi)$ has to be ignored, then

$$\nabla_r^T(\nabla_r\phi) = \sum_{i=1}^{N}\frac{\psi_i}{\sigma_i^2}exp\left[-\frac{(\boldsymbol{r}-\boldsymbol{r}_{obsi})^T N_i(\boldsymbol{r}-\boldsymbol{r}_{obsi})}{\sigma_i}\right]\cdot \left[2N_i(\boldsymbol{r}-\boldsymbol{r}_{obsi})(\boldsymbol{r}-\boldsymbol{r}_{obsi})^T N_i - \sigma_i N_i\right] \tag{34}$$

We can choose $\ddot{\boldsymbol{r}}$ to be

$$\ddot{\boldsymbol{r}} = -k\nabla_r^T(\nabla_r\phi)\dot{\boldsymbol{r}} - k\nabla_{r_{obsi}}^T(\nabla_r\phi)\dot{\boldsymbol{r}}_{obsi} - K_d(k\nabla_r\phi + \dot{\boldsymbol{r}}) \tag{35}$$

where K_d is a diagonal positive matrix.

Substituting $\ddot{\boldsymbol{r}}$ into (31) and yields

$$\dot{V}_2 = -(k\nabla\phi + \dot{\boldsymbol{r}})^T K_d(k\nabla\phi + \dot{\boldsymbol{r}}) \tag{36}$$

which is negative semi-definite and thus the system is stable.

Substituting $\ddot{\boldsymbol{r}}$ into (12) and solving for $\boldsymbol{u}_{APF}$ gives

$$\boldsymbol{u}_{APF} = -(k\nabla_r^T(\nabla_r\phi)\dot{\boldsymbol{r}} + k\nabla_{r_{obsi}}^T(\nabla_r\phi)\dot{\boldsymbol{r}}_{obsi} + K_d(k\nabla_r\phi + \dot{\boldsymbol{r}}) + A_c\boldsymbol{x}) \tag{37}$$

Where $A_c = [A_{21}\ A_{22}]$.

Hence, the overall OSMC/APF control effort is

$$\boldsymbol{u}(t) = \boldsymbol{u}_{osmc}(t) + \boldsymbol{u}_{APF} \tag{38}$$

IV. Numerical Results and Analysis

The purpose is to force the chaser vehicle from some initial state to a desired state while collision with obstacles is avoided. The initial orbit elements of the target spacecraft are shown in TABLE I.

TABLE I. Orbit elements of target spacecraft

Orbit elements	a(km)	e	$i(^\circ)$	$\omega(^\circ)$	$\Omega(^\circ)$	$f(^\circ)$
Values	6378.137	0.05	30	60	0	0

The initial relative conditions of the chaser spacecraft are set to be

$$\begin{cases} \boldsymbol{r}_0 = (200\ \ 400\ \ 200)^T \text{m} \\ \dot{\boldsymbol{r}}_0 = (0\ \ 0\ \ 0)^T \text{m/s} \end{cases} \tag{39}$$

The initial states of moving obstacles are

$$\begin{cases} \boldsymbol{r}_{obs10} = (118.2\ \ 257\ \ 86.93)^T \text{m} \\ \dot{\boldsymbol{r}}_{obs10} = (0\ \ -0.2\ \ 0.1)^T \text{m/s} \\ \boldsymbol{r}_{obs20} = (58.44\ \ 92.47\ \ 58.42)^T \text{m} \\ \dot{\boldsymbol{r}}_{obs20} = (-0.05\ \ 0.01\ \ 0)^T \text{m/s} \end{cases} \tag{40}$$

and the radius of spherical envelope:

$$R_{obs1} = 20\text{m},\ R_{obs2} = 15\text{m} \tag{41}$$

For optimal sliding mode controller, these weighted matrixes are selected to be

$$Q = diag(10^3, 10^4, 10^3, 5\times10^5, 5\times10^5, 5\times10^5) \tag{42}$$

$$R = 5\times diag(10^6, 10^6, 10^6) \tag{43}$$

$$K = 2\times diag(10^{-2}, 10^{-2}, 10^{-2}) \tag{44}$$

The value of α is $\alpha = 0.9$ and $\varepsilon = 1e^{-4}$.

Parameters for APF controller are selected to be

$$N_i = 5\times diag(e^{-3}, e^{-3}, e^{-3}) \tag{45}$$

$$M_i = 8\times diag(e^{-2}, e^{-2}, e^{-2}) \tag{46}$$

$$K_d = 5\times diag(1e^{-2}, 1e^{-2}, 1e^{-2}) \tag{47}$$

the value of k and σ_i are selected to be $k = 1$, $\sigma_i = 1$. The selection of ψ_i values are computed to guarantee collision avoidance, a sufficient but not necessary criterion for collision avoidance is that $\phi|_{ob} \geq \phi_a(\boldsymbol{r}_0)$. The value of each ψ_i is chosen to enforce this criterion.

The parameters of J_2 perturbation and atmospheric drag of two spacecraft are selected to be

$$m_t = 400\text{kg},\ C_{dt} = 2,\ A_t = 2\text{m}^2,\ \rho_t = 10^{-10}\text{kg/m}^3 \tag{48}$$

$$m_c = 100\text{kg},\ C_{dc} = 2,\ A_c = 0.5\text{m}^2,\ \rho_c = 10^{-10}\text{kg/m}^3 \tag{49}$$

The set of results obtained for the constrained rendezvous are illustrated below. In the situation of unconstrained rendezvous, the optimal control trajectory depending on OSMC method is shown in Fig. 1. Under the circumstance of constrained rendezvous, the three dimensional trajectories generated by the OSMC method and OSMC/APF method are plotted in Fig. 2 and Fig. 3 respectively. In these cases, obstacles are moving with constant velocity and trajectories of two obstacles are represented with a sequences of small red circles. Once the distance between the obstacle and the chaser spacecraft is shortest, the envelope will be shown. The time histories of acceleration, position and velocity are displayed in Fig. 4, Fig. 5 and Fig. 6 respectively. The acceleration caused by SMC method and external disturbances are shown in Fig. 7 and Fig. 8.

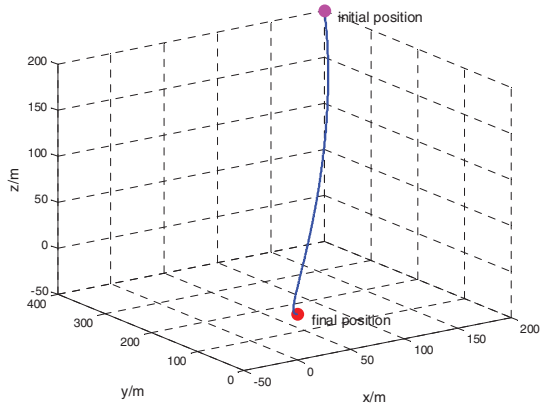

Fig. 1 Unconstrained Rendezvous using OSMC Method

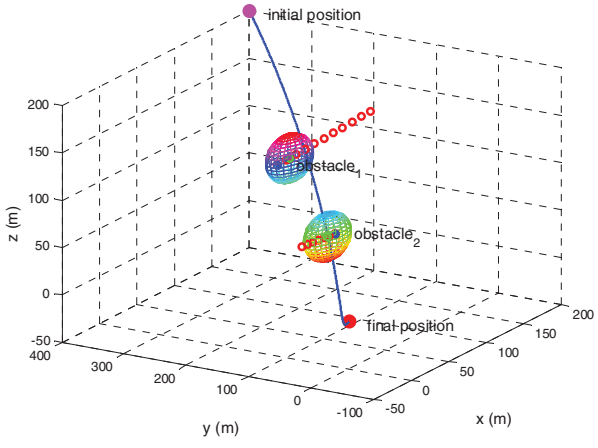

Fig. 2 Constrained Rendezvous using OSMC

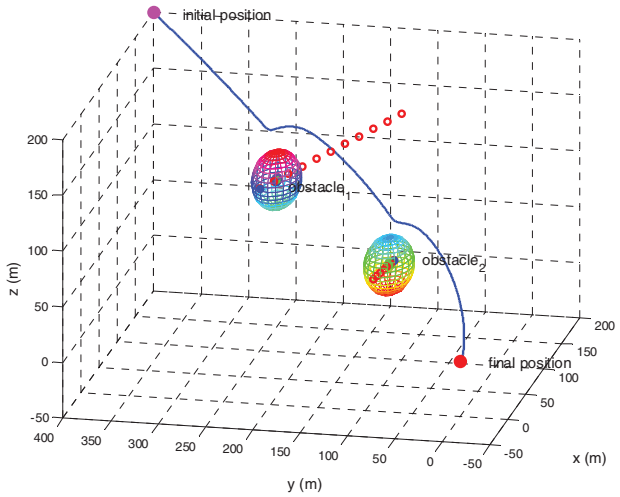

Fig. 3 Constrained Rendezvous using OSMC/APF Method

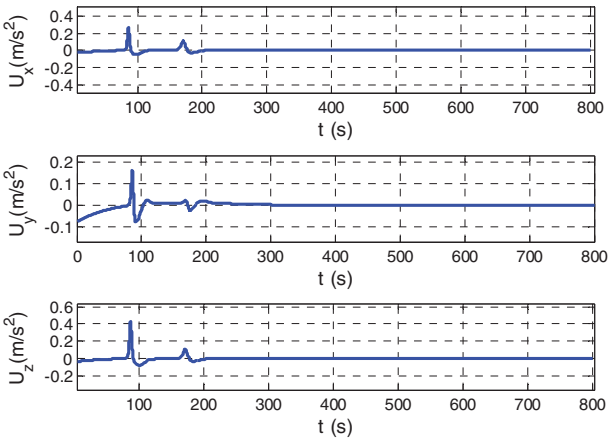

Fig. 4 Time History of Control Acceleration using OSMC/APF Method

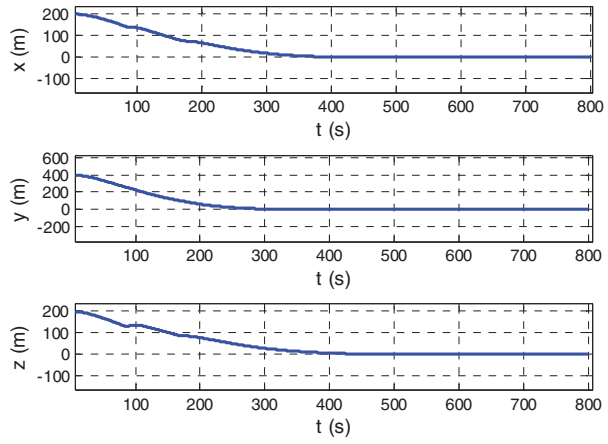

Fig. 5 Time History of Position using OSMC/APF Method

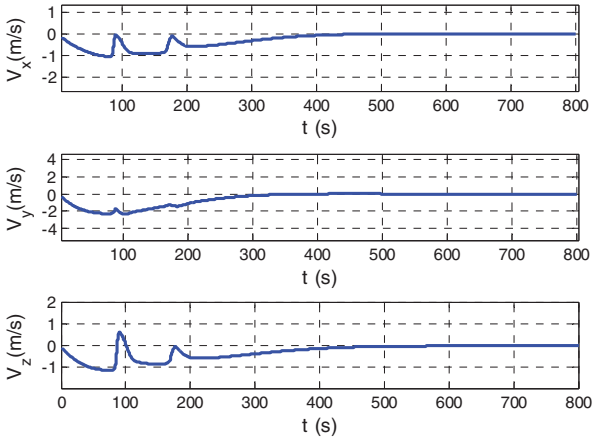

Fig. 6 Time History of Velocity using OSMC/APF Method

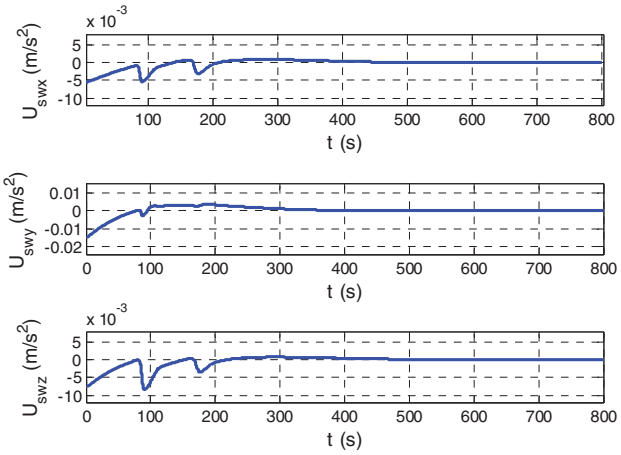

Fig. 7 Time History of Control Acceleration caused by SMC Method

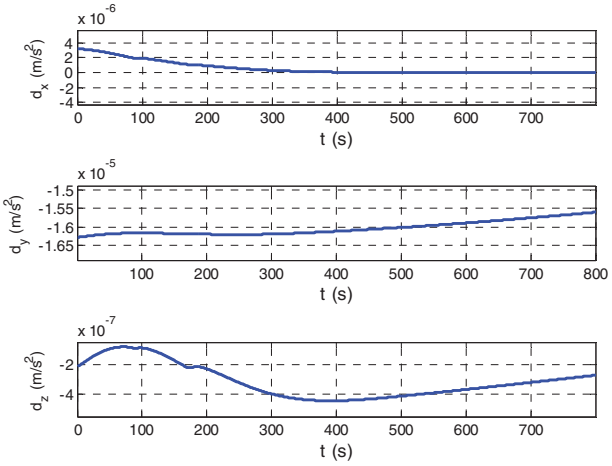

Fig. 8 Time History of Acceleration caused by External Disturbances

By comparison Fig. 2 and Fig. 3, it is easy to find that the proposed OSMC/APF algorithm successfully made the chaser spacecraft reach the desired point and while escaping collision with obstacles. In Fig. 4, it is obvious that the control acceleration changed dramatically around time 100s and 150s for the reason of avoiding moving obstacles. Fig. 5 illustrates that the relative position between the target and the chaser spacecraft decreased gradually and finally converged to zero. From Fig. 6, the relative velocity in three-axis soared to zero once the chaser spacecraft approached the boundary of obstacle and this coincided with the time history of acceleration. In the whole rendezvous period, the relative velocity fluctuated when the chaser spacecraft was close to obstacles and finally converged to zero. By analyzing Fig. 7 and Fig. 8, the function of disturbances are obvious before 300s and the acceleration caused by SMC method supports this, hence the designed optimal sliding mode controller is useful.

V. CONCLUSION

In this study, a novel method was introduced which utilized the nonlinear dynamics of a system to develop a nonlinear optimal control scheme with collision avoidance. The proposed control strategy includes two parts: optimal sliding mode control and APF control. The optimal sliding mode controller was designed based on the state-dependent Riccatic equation, and then integral sliding mode technique was utilized to deal with parameter uncertainty and external disturbance. The designed APF controller took velocity of both the chaser and obstacle into consideration and the attractive part of original APF controller was replaced by the optimal sliding mode controller. Only J_2 perturbation and atmospheric drag were considered as external disturbance. The global stability of the closed-loop system was proved by Lyapunov second method. Simulation results showed effective and robust performance of the proposed OSMC/APF combined controller in spacecraft close-range rendezvous process.

REFERENCES

[1] W. Fehse, Automated tendezvous and docking of spacecraft, First ed., New York: Cambridge University, 2003.

[2] D. C. Redding, N. J. Adams, and E. T. Kubiak, "Linear-quadratic station-keeping for the STS orbiter," Journal of Guidance, Control, and Dynamics, vol. 12, pp. 248-564, 1989.

[3] V. Kapila, A. G. Sparks, J. M. Buffington, and Q. Yan, "Spacecraft formation flying: dynamics and control," Journal of Guidance, Control, and Dynamics, vol. 23, no. 3, pp. 561-564, 2000.

[4] P. K. Menon, T. Lam, L. s. Crawford, and C. V. H. L, "Real-time computational methods for SDRE nonlinear control of missiles," in American Control Conference, AK, 2002, pp. 232-237.

[5] T. Cimen, "Survey of state-dependent Riccati equation in nonlinear optimal feedback control synthesis," Journal of Guidance, Control, and Dynamics, vol. 35, no. 4, pp. 1025-1047, 2012.

[6] J. R. Cloutier, C. N. D'Souza, and C. P. Mracek, "Nonlinear regulation and nonlinear Hinf control via the state-dependent Riccati equation technique," in Proceedings of the First International Conference on Nonlinear Problems in Aviation and Aerospace, Daytona Beach, Florida, 1996.

[7] D. T. Stansbery, and J. R. Cloutier, "Position and Attitude Control of Spacecraft Using the State-Dependent Riccati Equation Technique," in Proceedings of the 2000 American Control Conference, Chicago, USA, 2000, pp. 1867-1871.

[8] M. Mauro, and Z. Matti, "Application of SDRE technique to orbital and attitude control of spacecraft formation flying," Acta Astronautica, vol. 94, pp. 409-420, 2014.

[9] V. Utkin, "Variable structure systems with sliding modes," Automatic Control, IEEE Transactions on, vol. 22, no. 2, pp. 212-222, 1977.

[10] H. H. Yeh, E. Nelson, and A. Sparks, "Nonlinear tracking control for satellite formations," Journal of Guidance, Control, and Dynamics, vol. 25, no. 2, pp. 376-386, 2002.

[11] L. Hui, L. Junfeng, and H. Baoying, "Sliding mode control for low-thrust earth-orbiting spacecraft formation maneuvering," Aerospace Science and Technology, vol. 10, no. 7, pp. 636-643, 2006.

[12] J. Bae, and Y. Kim, "Adaptive controller design for spacecraft formation flying using sliding mode controller and neural networks," Journal of the Franklin Institute, vol. 349, pp. 578-603, 2012.

[13] L. Cao, X. Q. Chen, and A. K. Misra, "Minimum sliding mode error feedback control for fault tolerant reconfigurable satellite formations with J2 perturbations," Acta Astronautica, vol. 96, no. 201-216, 2014.

[14] M. Basin, P. Rodriguez-Ramirez, A. Ferrara, and D. Calderon-Alvarez, "Sliding mode optimal control for linear systems," Journal of the Franklin Institute, vol. 349, no. 4, pp. 1350-1363, 5//, 2012.

[15] M. Das, and C. Mahanta, "Optimal second order sliding mode control for linear uncertain systems," ISA Transactions, vol. 53, no. 6, pp. 1807-1815, 11//, 2014.

[16] A. Imani, M. Bahrami, and B. Ebrahimi, "Optimal sliding mode control for spacecraft formation flying." pp. 38-43.

[17] C. Pukdeboon, and A. S. I. Zinober, "Optimal sliding mode controllers for attitude tracking of spacecraft." pp. 1708-1713.

[18] A. Imani, and B. Borhan, "Robust control of spacecraft rendezvous on elliptical orbits: Optimal sliding mdoe and backstepping sliding mode approaches," Journal of Aerospace Engineering, vol. 0, no. 0, pp. 1-15, 2015.

[19] O. Khatib, "Real-time obstacle avoidance for manipulators and mobile robots," Internaltional Journal of Robotics Research, vol. 5, no. 1, pp. 90-99, 1986.

[20] I. Lopze, and C. R. McInnes, "Autonomous rendezvous using artificial potential function guidance," Journal of Guidance, Control, and Dynamics, vol. 18, no. 2, pp. 237-241, 1995.

[21] M. T. Wolf, and J. Burdick, "Artificial potential functions for highway driving with collision avoidance," in IEEE International Conference on Robotics and Automation, 2008.

[22] T. Chen, H. Wen, H. Hu, and D. Jin, "Output consensus and collision avoidance of a team of flexible spacecraft for on-orbit autonomous Assembly," Acta Astronautica.

[23] Q. Hu, H. Dong, Y. Zhang, and G. Ma, "Tracking control of spacecraft formation flying with collision avoidance," Aerospace Science and Technology, vol. 42, pp. 353-364, 4//, 2015.

[24] L. Palacios, M. Ceriotti, and G. Radice, "Close proximity formation flying via linear quadratic tracking controller and artificial potential function," Advances in Space Research, vol. 56, no. 10, pp. 2167-2176, 11/15/, 2015.

[25] J. D. Munoz, "Rapid path-planning algorithm for autonomous proximity operations of satellites," University of Florida, 2011.

[26] P. Gao, and J. J. Luo, "Adaptive artificial potential function guidance for dynamic obstacle avoidance of spacecraft," Chinese Space Science and Technology, 2012.

[27] R. Bevilacqua, T. Lehmann, and M. Romano, "Development and experimentation of LQR/APF guidance and control for autonomous proximity maneuvers of multiple spacecraft," Acta Astronautica, vol. 68, no. 7–8, pp. 1260-1275, 4//, 2011.

[28] S. B. McCamish, and M. Romano, "Flight testing of multiple-spacecraft control on SPHERES during close-proximity operations," Journal of Spacecraft and Rockets, vol. 46, no. 6, pp. 1202-1213, 2009.

[29] J. M. Daniel, "Swarm keeping strategies for spacecrft under J2 and atomospheric drag perturbations," Aerospace Engineering University of Illinois at Urbana-Champaign, 2011.

[30] D. Lee, H. Bang, E. A. Butcher, and A. K. Sanyal, "Nonlinear output tracking and disturbance rejection for autonomous close-range rendezvous and docking of spacecraft," Transactions of the Japan Society for Aearonautical and Space Science, vol. 57, no. 4, pp. 225-237, 2014.

[31] R. Andre Fields, "Continuous Control Artificial Potential Function Methods and Optimal Control," Department of Aeronautics and Astronautics, Air Force Institute of Technology Air University, 2014.